Kairos: Soil-Aware Transmission Control For Long-Term Agricultural Cross-Soil LoRa

Jingkai Lin*, Yidong Ren†, Jialuo Du*, Yimeng Liu*, Yawen Wang*, Younsuk Dong*, Tianxing Li*, Zhichao Cao*
*Michigan State University, East Lansing, MI, USA †Qualcomm, Santa Clara, CA, USA
Email: {linjingk, dujialuo, liuyime2, wangyaw5, dongyoun, litianx2, caozc}@msu.edu, yidoren@qti.qualcomm.com

***Abstract*—LoRa, a widely adopted low-power wide-area Internet-of-Things (IoT) paradigm, has demonstrated its potential to enable cross-soil communication, in which LoRa antennas are buried in the soil, thereby benefiting smart agriculture. Unlike LoRa links in the air, cross-soil links are highly dynamic due to the frequent changes in soil conditions. Thus, we need to tune their configurations to ensure long-term communication. Unfortunately, we find that the default periodical adjustment cannot handle complex environment changes, degrading energy efficiency. In this paper, we present Kairos, a soil-aware transmission control scheme that optimizes the overall energy efficiency of cross-soil LoRa communication. The main idea of Kairos is to predict the recoverable polarization gain and trigger calibration when it can reduce data-transmission energy. It then minimizes the probing overhead required to identify a suitable polarization state. First, we develop an energy model to estimate transmission cost across link configurations and use it to determine when calibration is worthwhile. We further design an efficient configuration-search algorithm to reduce probing overhead and a transmission-management mechanism for adaptive parameter tuning between the node and gateway. We implement Kairos using commercial off-the-shelf devices and evaluate its performance in an agricultural field. Extensive experimental results show that Kairos reduces energy consumption by up to $3.71\times$ compared to state-of-the-art solutions.**

***Index Terms*—LPWAN, LoRa, Cross-soil Communication**

I. Introduction

The Internet of Things (IoT) is increasingly important for precision agriculture [1]–[5], enabling real-time monitoring of soil moisture, weather, vegetation, and other environmental factors. Soil monitoring is particularly critical for evaluating irrigation effectiveness and supporting data-driven agricultural decisions. While commercial systems typically place sensors underground and communication modules aboveground, fully underground deployment is becoming desirable to reduce interference with seeding, irrigation, fertilization, pest control, and harvesting [6]–[8]. This trend makes cross-soil communication a key challenge for agricultural IoT [9]–[11].

LoRa is well suited for agricultural IoT because of its low power consumption and long communication range [12]–[15]. Existing moisture-aware transmission-control methods [16] adapt link configurations to compensate for moisture-induced attenuation, but they typically assume a fixed antenna state and overlook polarization mismatch. Recent work, Demeter [17], introduces a polarization-programmable LoRa antenna compatible with commercial nodes to improve cross-soil communication. Since soil propagation causes strong polarization dynamics, signal quality can degrade when transmitter and receiver antennas are misaligned. Demeter addresses this issue by using a programmable phase shifter to probe different polarization states and identify a better alignment.

979-8-3195-0662-7/26/$31.00 © 2026 IEEE

However, our measurements show that the timing of polarization calibration is critical to energy efficiency. Each calibration round requires probing packets, introducing non-negligible overhead. Determining the optimal timing is challenging: frequent periodic calibration wastes energy, while infrequent calibration can cause severe polarization misalignment and force the node to use more energy-intensive LoRa settings, such as larger spreading factors. Simple soil-moisture-based heuristics are also ineffective, since polarization may vary significantly under the same soil moisture condition at different times. Therefore, polarization calibration should be integrated with energy-aware transmission control rather than treated as a standalone operation.

In this paper, we propose **Kairos**, a polarization-aware transmission control scheme for cross-soil LoRa communication. Unlike traditional LoRa control, which mainly adapts parameters such as spreading factor and transmission power, Kairos integrates polarization calibration into the control loop to improve energy efficiency under dynamic soil conditions. Kairos addresses three key questions: 1) when calibration can reduce data-transmission energy; 2) how to search polarization states with low overhead; and 3) how to integrate polarization-aware control into existing LoRa systems through distributed node-gateway coordination.

Challenge 1: *Energy Modeling under High Uncertainty.* Energy optimization requires estimating the cost and benefit of each transmission strategy. In cross-soil LoRa links, energy efficiency depends jointly on polarization, spreading factor (SF), transmission power (TP), soil moisture, and link dynamics [18]. Moreover, the benefit of calibration depends on future transmissions, which are difficult to predict. This makes it challenging to determine when calibration is worth its energy cost.

Challenge 2: *Energy-aware Polarization Search.* A cross-soil LoRa node can select from many discrete polarization states over 360°. Exhaustive search is costly, while random probing may be inefficient and miss good alignments. The large search space and time-varying soil channel make fast, energy-aware polarization search difficult in practice.

Challenge 3: *Compatibility with Existing LoRa Control.* LoRaWAN already supports transmission control mechanisms, such as Adaptive Data Rate (ADR), where gateways adjust SF and TP based on link conditions. However, existing control does not consider antenna polarization. Adding polarization-aware control, therefore, requires coordination between nodes and gateways while preserving LoRa's lightweight, distributed design.

To address these challenges, Kairos introduces three key components.

First, Kairos develops a threshold-based energy estimation model that predicts transmission cost under different SNR and SF settings and derives the minimum SNR gain required for calibration to reduce energy consumption. A soil-aware margin prediction model then estimates the polarization-optimized SNR under the current Volumetric Water Content (VWC) and compares it with the measured current SNR. Calibration is triggered only when the predicted recoverable margin enables a more energy-efficient transmission configuration.

Second, Kairos designs a history-guided polarization search strategy to reduce probing overhead. It first probes the historically best direction under similar soil moisture as a warm start, and then applies a lightweight heuristic search within a local interval when further refinement is needed. Kairos also uses an energy-aware stopping rule that terminates probing once the observed SNR is sufficient to support the minimum-cost transmission setting, avoiding unnecessary calibration cost.

Third, Kairos introduces a polarization-aware transmission mechanism that coordinates the node and gateway. The node maintains reliability by using conservative settings after packet loss, while the gateway schedules calibration and recommends energy-efficient parameters using current and historical link conditions.

We implement Kairos using commercial-off-the-shelf (COTS) LoRa devices and soil moisture sensors, and evaluate it in a soybean field. The results show that Kairos reduces energy consumption by up to 3.71× compared with state-of-the-art solutions.

The main contributions of this work are:

- We design Kairos, a polarization-aware transmission control protocol that determines when and how to adjust transmission settings to improve the energy efficiency of LoRa cross-soil communication.
- We develop a threshold-based energy estimation model and a margin prediction model to trigger calibration when the predicted recoverable SNR gain enables a more energy-efficient transmission configuration.
- We implement Kairos with COTS LoRa devices and evaluate it in a soybean field, showing up to 3.71× energy reduction over state-of-the-art solutions.

II. Preliminary and Empirical Study

A. LoRa Physical Layer and Cross-Soil LoRa

LoRa uses Chirp Spread Spectrum (CSS) modulation [19]–[25], where each symbol is represented by a chirp whose initial frequency encodes data bits. The SF controls the tradeoff between data rate and noise resistance. The symbol duration is:

$$T = \frac{2^{SF}}{BW} \tag{1}$$

where BW is the bandwidth. Since each symbol carries SF bits, the LoRa data rate is:

$$DR = \frac{SF \cdot BW}{2^{SF}} \tag{2}$$

LoRaWAN v1.0.3 (US915) uses uplink SFs from 7 to 10 by default. With a fixed BW, a larger SF increases symbol duration and improves noise resistance, but lowers data rate and increases energy cost per bit [26]–[28].

When LoRa nodes are buried underground and communicate with above-ground gateways, soil introduces stronger link dynamics than in-air propagation. Higher soil moisture increases attenuation [17], while the heterogeneous and lossy soil medium causes scattering, reflection, and refraction. These effects alter the signal polarization and can create receiver-side polarization misalignment even with preconfigured antennas [17]. Meanwhile, directly applying advanced antennas (e.g., dual-polarization, circular-polarization, and directional antennas) remains inefficient in terms of COTS compatibility, reliability, polarization self-alignment, and low overhead [17]. Demeter [17] addresses this issue with a programmable LoRa antenna compatible with low-cost COTS nodes. Each antenna uses a phase shifter to adjust the polarization direction, supporting 45 discrete configurations that cover the full 360° polarization range.

Therefore, for cross-soil LoRa communication, both selecting an appropriate SF and timely calibrating polarization based on channel quality are essential for balancing packet delivery reliability, retransmission cost, and node battery lifetime.

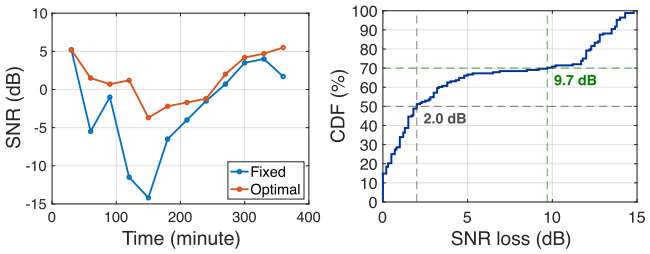

(a) Short Term (b) Long Term

Fig. 1: SNR comparison between a fixed polarization direction and the optimal one.

B. Empirical Study of Polarization Calibration

To understand the importance and challenges of polarization calibration, we conduct an empirical study of cross-soil links in a real-world soybean field during the growing season. A LoRa node equipped with a Demeter antenna is buried 40 cm underground and configured to sequentially transmit signals across all 45 polarization directions. A COTS LoRa gateway is positioned 60 meters away, at a height of 2 meters, to receive packets. The data collection lasts 7 days and covers diverse weather and soil conditions.

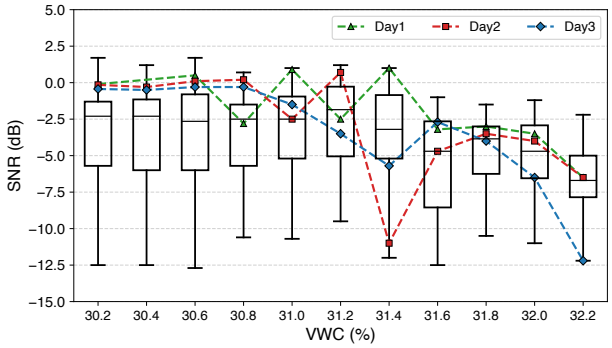

Fig. 2: The five value bars indicate SNR variation across all polarization directions under different VWC levels over three days. The lines indicate SNR variation, giving a specific polarization direction.

Figure 1 shows that polarization misalignment can cause severe and persistent SNR loss. In Figure 1(a), the optimal polarization direction changes over time as soil conditions evolve. Therefore, a fixed polarization direction can quickly become suboptimal. Around the 150th minute, the fixed direction suffers more than 10 dB SNR loss compared with the optimal direction. Figure 1(b) further shows that such degradation is not occasional. Across the 7-day trace, 50% of SNR losses exceed 2 dB, and 30% exceed 9.7 dB. These results indicate that long-term cross-soil LoRa links cannot rely on a fixed polarization direction. Without timely polarization calibration, the node may have to use a larger spreading factor or retransmit lost packets, both of which directly increase energy consumption.

These observations reveal that energy-efficient polarization adaptation involves two distinct subproblems. The first is *when to trigger polarization calibration*. The second is *how to find a suitable polarization direction efficiently once calibration is triggered*. We discuss them separately below.

When to trigger polarization calibration. A fixed strategy that never recalibrates is insufficient because cross-soil polarization drift can accumulate and cause large SNR losses. Periodic calibration, as used by Demeter, provides a straightforward alternative, but it is difficult to tune because polarization dynamics do not follow a fixed time scale. A long period may miss rapid SNR drops, while a short period wastes energy on unnecessary probing.

An adaptive approach is to trigger calibration based on soil moisture variation, since moisture strongly affects underground propagation. For example, calibration can be invoked when the VWC difference from the last calibration exceeds a threshold. However, this policy still assumes that VWC variation reliably indicates steady variation in link quality, which is not always the case. Given a polarization setting, VWC and SNR variations are not linear or one-to-one: a small change in moisture may cause a large SNR drop, while similar moisture changes may lead to different SNR responses.

Figure 2 illustrates this mismatch by showing the SNR variation of a fixed polarization direction under different VWC levels over three days. The key observation is that the fixed-polarization SNR does not vary smoothly or uniquely with VWC. For example, on Day 2, increasing VWC from 31.2% to 31.4% is accompanied by an 11.7 dB SNR drop, whereas similar VWC changes at lower moisture levels produce little variation. Moreover, at the same VWC of 31.4%, the measured SNR differs substantially across days. These results indicate that VWC alone cannot reliably predict the instantaneous SNR under a fixed polarization state, because the observed link quality also depends on time-varying polarization mismatch.

This limitation motivates an energy-aware trigger that initiates calibration only when the predicted recoverable polarization gain can reduce data-transmission energy, rather than relying on elapsed time or VWC variation alone.

How to find a suitable polarization direction efficiently. Once calibration is triggered, the node must determine which polarization direction to use. A naive solution is to exhaustively probe all candidate directions, but this incurs high overhead, especially under dynamic conditions such as rainfall or irrigation where recalibration may be frequent. In such cases, probing many directions before each data transmission can dominate the total energy consumption.

To reduce search overhead, a straightforward alternative is to reuse historical calibration results, such as selecting the best direction previously observed at the same soil moisture level. However, history-based lookup alone is not always reliable because the same VWC value may correspond to different polarization responses over time. Figure 2 illustrates this through a vertical comparison at VWC = 31.4%, where the SNRs of the same polarization direction on Day 1, Day 2, and Day 3 are 1.0 dB (Optimal), -11 dB, and -5.7 dB, respectively. This large variation shows that the same moisture level does not necessarily imply the same link quality or the same suitable polarization direction.

These observations motivate an efficient online search strategy that uses historical results as guidance, rather than directly trusting them, to find a suitable polarization direction with low probing overhead.

Motivation: In summary, energy-efficient cross-soil LoRa communication requires jointly deciding *when* to trigger polarization calibration and *how* to identify a suitable direction with low overhead. Fixed, periodic, and moisture-threshold triggers may miss energy-saving opportunities, while historical lookup alone can fail under time-varying polarization responses. These observations motivate Kairos to jointly optimize calibration triggering and polarization search, triggering calibration when the predicted recoverable gain can reduce data-transmission energy and minimizing the probing overhead during calibration.

III. Design

A. Design Overview

Kairos is a polarization-aware transmission control framework that reduces energy consumption in cross-soil LoRa networks by jointly managing antenna polarization and transmission parameters. As shown in Figure 3, Kairos follows a distributed design aligned with the LoRaWAN paradigm,

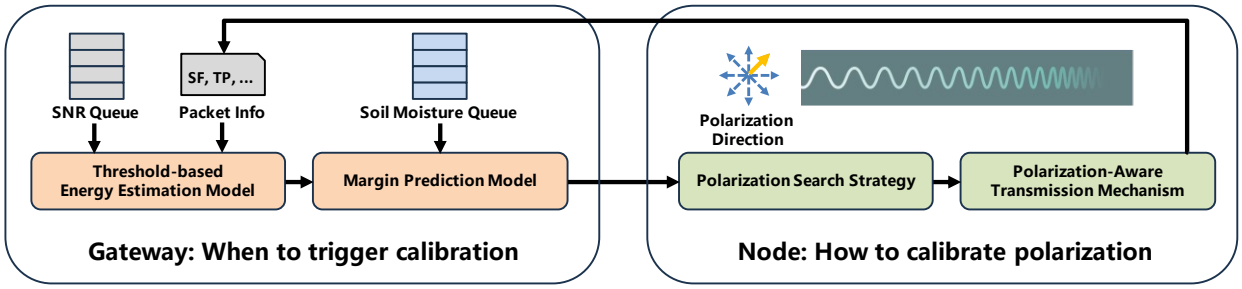

Fig. 3: Overview of Kairos. At the gateway, the threshold-based energy estimation model and the margin prediction model determine when to trigger a transmission calibration. At the node, the polarization search strategy and the polarization-aware transmission mechanism determine how to transmit probes and data packets efficiently.

TABLE I: Important notation and description

Notation	Description
DR	Data rate determined by the spreading factor SF.
SNR	Signal-to-noise ratio measured for a received packet.
$P_{preamble}$	Probability of successful preamble detection.
P_h	Probability of successful decoding of the header.
P_p	Probability of successful decoding of the payload.
Δ_{soil}	Empirical correction for PDR-model mismatch.
σ	SNR gain threshold to trigger polarization calibration.
SNR_0	Baseline SNR observed before polarization calibration.
EC	Energy cost over a calibration cycle.
TC	Expected transmission energy per payload bit.

where gateways make control decisions, and nodes execute calibration actions. Table I summarizes the key notations and parameters used throughout the design. On the gateway side, Kairos determines when polarization calibration should be triggered. The gateway aggregates SNR measurements, packet information, and soil moisture data, and applies a threshold-based energy estimation model to assess whether calibration can enable more energy-efficient transmission (§ III-C). To implement the threshold-based energy estimation model over a cross-soil link, a margin prediction model then estimates the achievable SNR improvement after calibration and triggers calibration only when the predicted margin exceeds the corresponding threshold (§ III-D). On the node side, Kairos determines how calibration is performed. The node employs an efficient polarization-search strategy to minimize probing overhead (§ III-E) and a polarization-aware transmission mechanism to manage packet retransmissions under dynamic channel conditions (§ III-F). Together, these components enable energy-efficient and reliable cross-soil communication with minimal changes to existing LoRa operation.

B. Problem Description

Goal. The overall objective of Kairos is to minimize the Energy Cost (EC) of long-term cross-soil LoRa communication, which includes both the polarization calibration overhead and the energy cost of data transmission. To analyze EC, we first define the Transmission Cost (TC) as the expected energy cost of delivering a data packet:

$$TC(SNR, SF) = \frac{TP}{DR(SF) \cdot PDR(SNR, SF)} \tag{3}$$

where SNR denotes the received SNR at the gateway, and PDR is jointly determined by SNR and SF. This formulation accounts for both the initial transmission and potential retransmissions.

Since data packets are transmitted continuously, TC dominates long-term energy consumption and is the primary target for minimizing EC. In contrast, polarization calibration is performed intermittently and introduces additional overhead that must be justified by its impact on TC reduction.

We define a periodic calibration cycle, at the beginning of which Kairos decides whether calibration is needed. The EC includes the K probing packets used for calibration and the following n data packets generated within the cycle. If calibration is not triggered, $K = 0$. The total EC over the calibration cycle is:

$$EC(K, SF) = \frac{q \cdot TP}{DR(SF)} \cdot K + p \cdot \sum_{i=1}^{n} TC(SNR_i + H(K), SF), \tag{4}$$

where p and q are the data and probing payload lengths, respectively. SNR_i denotes the SNR of the i-th distinct data packet without calibration, and $H(K)$ is the SNR gain achieved using K probes. The transmission cost TC already accounts for possible retransmissions through the PDR. Soil moisture and cross-soil channel are assumed to remain stable during the short calibration process.

According to Equation 4, to minimize EC, calibration is needed only when the energy savings in data transmission (i.e., the latter term) exceed the probing overhead (i.e., the former term). In practice, however, the total number of probes required is difficult to estimate under unpredictable cross-soil channels (§ II-B). To make the optimization tractable, we split it into two parts. First, we minimize the data-transmission energy: if the estimated optimal configuration under the current cross-soil channel provides an energy benefit, calibration is triggered. Second, we minimize the number of probes required during calibration.

C. Threshold-based Energy Estimation Model

The first task of Kairos is to determine when polarization calibration can reduce the expected transmission cost (TC). To this end, Kairos models the relationship between SNR, SF, data rate (DR), and packet delivery ratio (PDR).

For a given SF, the data rate is derived from the bandwidth and SF as shown in Equation 2. To estimate PDR, we model a LoRa packet as the combination of preamble, physical header, and payload. The overall PDR is given by the product of their decoding success probabilities [18]:

$$PDR(SNR, SF) = P_{preamble} \times P_h \times P_p. \tag{5}$$

The probability of preamble detection is modeled as:

$$P_{preamble} = 1 - P_b(SNR, SF + \log_2(m + 4.25)). \tag{6}$$

where m is the configured number of preamble symbols, $m + 4.25$ is the effective LoRa preamble length, and the logarithmic term captures the processing gain from repeated preamble chirps [29].

For a physical header with length L_h, the header decoding probability is:

$$P_h(SNR, SF) = \left((1 - P_b)^4 + 3(1 - P_b)^7 P_b\right)^{\left\lceil \frac{L_h}{4SF} \right\rceil}. \tag{7}$$

For an L_p-bit payload, the decoding probability is:

$$P_p(SNR, SF) = (1 - P_b)^{\left\lceil \frac{L_p}{SF} \right\rceil}. \tag{8}$$

Here, P_b denotes the LoRa symbol-error probability. It is analytically derived under the AWGN assumption using the Q-function [30]:

$$P_b(SNR, SF) = 0.5 \times Q\left(\sqrt{10^{SNR/10} \cdot 2^{SF+1}} - \sqrt{1.386 \cdot SF + 1.154}\right). \tag{9}$$

However, underground LoRa propagation deviates from the AWGN assumption. Soil absorption, non-Gaussian fading, and polarization misalignment introduce additional SNR degradation, causing the analytical model to overestimate the actual PDR. To account for this gap, Kairos introduces an empirical soil-induced degradation term Δ_{soil}:

$$P_b'(SNR, SF) = P_b(SNR - \Delta_{soil}, SF). \tag{10}$$

Here, Δ_{soil} captures the aggregate discrepancy between the analytical model and measured cross-soil links. It is fitted using an independent calibration trace and remains fixed during evaluation.

With the mapping from SNR and SF to DR and PDR, Kairos derives an SNR gain threshold for calibration. For n packets transmitted in a calibration cycle with spreading factor SF and initial SNR SNR_0, the expected transmission cost before calibration is:

$$TC_{\text{before}} = \frac{n}{DR(SF) \cdot PDR(SNR_0, SF)}. \tag{11}$$

After polarization calibration, if the SNR increases by σ and the node switches to $SF - 1$, the expected transmission cost becomes:

$$TC_{\text{after}} = \frac{n}{DR(SF - 1) \cdot PDR(SNR_0 + \sigma, SF - 1)}. \tag{12}$$

Kairos defines the required SNR gain threshold as the minimum σ that satisfies:

$$TC_{\text{after}} \leq TC_{\text{before}}. \tag{13}$$

D. Margin Prediction Model

To apply the threshold-based energy estimation model in cross-soil links, Kairos employs a margin prediction model to determine whether calibration can provide sufficient SNR improvement under the current soil condition. Kairos does not use VWC to predict the instantaneous SNR under the active polarization, which is also affected by time-varying polarization mismatch. Instead, it uses VWC to estimate the polarization-optimized SNR achievable after calibration. The key is to model soil-dependent path loss as a function of VWC.

We model soil-moisture-dependent path loss using the Peplinski dielectric model [31], which is widely used for underground wireless propagation at 0.3–1.3 GHz [16], [32].

The Margin Prediction Model uses VWC to estimate the path loss through the following three stages:

1) Estimating the complex dielectric constant. Based on the Peplinski model, the complex dielectric constant ε_{soil} of the soil is first estimated. To facilitate the computation of the propagation constant, we adopt an approximate square root form of ε_{soil}:

$$\sqrt{\varepsilon_{\text{soil}}} = 1.15\left[1 + \rho_b\left(\varepsilon_s^{0.65} - 1\right) + \text{VWC}^{0.65}\left(\varepsilon_{fw}^{0.65} - 1\right)\right]^{0.68} - j \cdot \left(\frac{\sigma_{\text{eff}}}{2\pi f \varepsilon_0}\right) \tag{14}$$

In this formulation, ρ_b denotes the soil bulk density, which can be obtained from site-specific measurements or soil classification tables. ε_s and ε_{fw} represent the dielectric constants of dry soil particles and free water, respectively, and are assigned empirical values, e.g., $\varepsilon_s = 4.7$ and $\varepsilon_{fw} = 80.1$ at room temperature. The effective conductivity σ_{eff} captures conductivity loss associated with soil composition, salinity, and moisture, and is calibrated from an independent site-specific trace before evaluation. The variable f denotes the signal frequency, and ε_0 is the vacuum permittivity.

2) Calculating the propagation constant. The complex propagation constant γ is then derived as:

$$\gamma = \alpha + j\beta = j \cdot \frac{2\pi f}{c} \cdot \sqrt{\varepsilon_{\text{soil}}} \tag{15}$$

Where c is the speed of light in vacuum, while α and β represent the attenuation and phase constants, respectively.

3) Computing the path loss. Finally, given the propagation distance d, the total path loss PL is calculated as:

$$PL = 20 \cdot \log_{10} e^{\alpha d} = 8.686 \cdot \alpha d \tag{16}$$

Using the estimated path loss, Kairos infers the polarization-optimized SNR under the current VWC from a reference measurement. It then computes the recoverable polarization margin as

$$\widehat{M} = \widehat{\text{SNR}}_{\text{opt}}(\text{VWC}) - \text{SNR}_{\text{current}}, \tag{17}$$

Where $\text{SNR}_{\text{current}}$ is measured under the active polarization state. Calibration is triggered only when $\widehat{M}$ exceeds the

energy-saving threshold derived in Section III-C. Thus, VWC provides a physical prior for the achievable post-calibration SNR rather than serving as a direct calibration trigger.

E. Polarization Search Strategy

After Kairos decides that calibration is necessary, it must find a suitable polarization direction with minimal probing overhead. Exhaustively probing all candidates is costly, so Kairos combines historical lookup with online refinement. It first retrieves the historically best direction under similar VWC and probes it as an opportunistic warm start, rather than assuming that VWC deterministically identifies the current optimal direction. If the probed direction already satisfies the energy-aware stopping condition, Kairos terminates calibration immediately. Otherwise, the measurement is reused as the first observation of the online search, and Kairos applies Golden Section Search (GSS) [33] within a local interval around that direction. Thus, an accurate historical direction can reduce the number of probes, while an inaccurate one does not introduce an additional probing round or increase the worst-case search budget. This hybrid strategy exploits historical observations when they remain valid, while still allowing online adaptation when VWC alone is insufficient. The search terminates according to an energy-aware stopping condition: once a probed direction provides enough SNR to support the minimum-cost transmission configuration derived earlier, Kairos stops immediately and uses it for data transmission, because further probing would only increase calibration cost without reducing the data-transmission cost.

F. Polarization-Aware Transmission Mechanism

Kairos is designed to be compatible with existing LoRa transmission control by following the ADR paradigm, where gateways perform control decisions while end devices remain lightweight. Rather than modifying ADR logic or MAC procedures, Kairos only requires minimal extensions to the uplink packet format, enabling the gateway to identify probing packets and associate link quality with the current polarization configuration.

Under this design, polarization-aware decisions are handled at the gateway, while nodes continue to rely on standard transmission and retransmission mechanisms. However, polarization-aware control fundamentally changes the role of retransmissions. Unlike conventional ADR, where retransmissions primarily serve reliability purposes, retransmissions in Kairos may be triggered either intentionally for energy efficiency or reactively due to channel degradation. As a result, retransmission management becomes a key component in ensuring both compatibility and energy efficiency.

The retransmission state can be divided into two subtypes: proactive retransmission, where the node deliberately chooses to retransmit using previously used parameters to conserve energy; and reactive retransmission, which is triggered by severe environmental fluctuations and involves increasing the SF to ensure reliable communication. Therefore, a key challenge in retransmission management lies in determining whether the current retransmission falls within the planned range.

Theorem 1. *The PDR after SF optimization exceeds half of the PDR observed before the adjustment.* Assume the SF before optimization is s, and the corresponding transmission cost is:

$$TC_s = \frac{1}{DR(s) \cdot PDR_s} \tag{18}$$

If we choose to reduce the SF to $s-1$, then the corresponding retransmission cost becomes:

$$TC_{s-1} = \frac{1}{DR(s-1) \cdot PDR_{s-1}} \tag{19}$$

Taking the ratio of the two expressions yields:

$$\frac{TC_{s-1}}{TC_s} = \left(\frac{1}{2} \times \frac{s}{s-1}\right) \times \frac{PDR_s}{PDR_{s-1}} \tag{20}$$

Since the final selected SF is $s-1$, it must hold that $TC_{s-1} < TC_s$. Therefore:

$$\frac{PDR_{s-1}}{PDR_s} > \frac{1}{2} \times \frac{s}{s-1} > \frac{1}{2} \tag{21}$$

In other words, the PDR after SF optimization remains above half of the value observed before the adjustment. □

Combined with Theorem 1, this implies that only the first retransmission can proactively reuse the reduced SF. If it fails, subsequent attempts must increase the SF to restore link margin and are therefore reactive. Since reducing SF is feasible only when the original link has substantial reliability margin, the pre-adjustment PDR is expected to be close to 100%, while Theorem 1 ensures that the optimized PDR remains above 50%. Hence, *only the first retransmission can be proactive; all subsequent retransmissions must be reactive.*

Based on this insight, we propose a hybrid retransmission strategy: the first retransmission reuses the SF before adjustment, while all subsequent retransmissions use a larger SF to ensure reliable communication.

G. Distributed Protocol Design

Figure 4 illustrates the interactions between the gateway and node. Upon receiving an uplink packet, the gateway identifies it as either a probe or a data packet. For a data packet, Kairos reads the current VWC and active-state SNR, and estimates the recoverable margin using prior calibration results and fixed model parameters. It then decides whether calibration is needed and, if so, which direction to probe. For a probing packet, the gateway records the SNR of the selected direction and returns feedback through the corresponding receive window. During trace-based evaluation, the evaluator reveals only the outcome of the selected action before Kairos updates its state; unselected directions and future measurements remain hidden.

The node operates in transmission-control and polarization-search states. It normally sends data using the assigned settings and manages retransmissions as described earlier. When instructed by the gateway, it probes candidate directions according to the search strategy. Together, these states enable lightweight and causal node–gateway coordination.

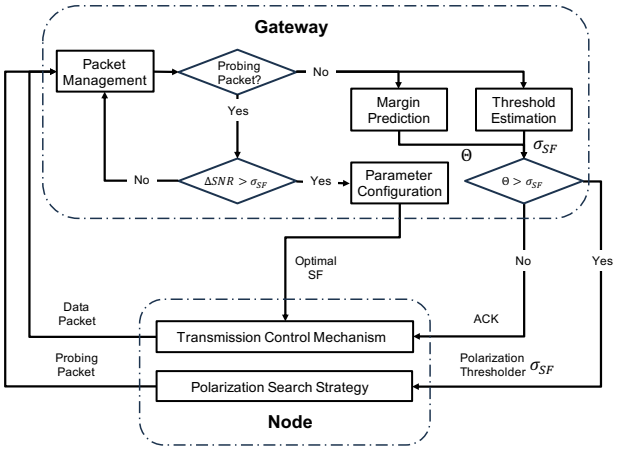

Fig. 4: The distributed protocol framework of Kairos at a gateway and a node.

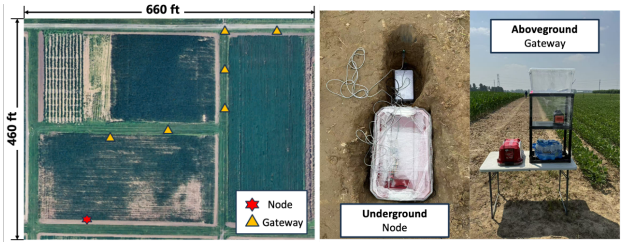

Fig. 5: Experiments deployment in a soybean farm

IV. Implementation and Evaluation

A. Implementation

We implement a cross-soil system to collect real-world link traces and replay Kairos and the baselines over the measured channel conditions. The system follows LoRaWAN 1.0.3 and employs a Dragino LPS8 gateway [34], a Dragino LoRa Shield v1.4 [35], and a PINO-TECH Soil Watch 10 sensor [36]. The underground node uses the programmable-polarization antenna developed in Demeter [17], including a passive RF splitter [37], a PE44820 digital phase shifter [38] with 45 phase settings, a hybrid coupler, and a dual-polarized antenna [39].

The node sequentially transmits over all 45 polarization directions and four SFs every 30 minutes, with the VWC included in the payload. These dense measurements provide the evaluator with the outcome of possible actions but are not directly exposed to the scheduling policies. During replay, each policy observes only the current VWC, the SNR under its active polarization state, prior observations, and fixed model outputs. After an action is selected, the evaluator returns only the corresponding trace measurement, unselected configurations and future samples remain hidden.

We collect traces over 15 days in a soybean field. For the main 7-day deployment, the node is buried 40 cm underground and the gateway is placed 60 m away at a height of 2 m. The trace covers varying weather, moisture, and temperature conditions, including rainfall on Days 2 and 6. During the remaining eight days, we vary the gateway distance and node depth to evaluate different deployment geometries.

The 7-day trace is used exclusively for the main energy evaluation and is not used for model fitting. Among the remaining eight days, one control day uses the same depth and distance as the main deployment and is used to calibrate the two site-specific parameters, Δ_{soil} and σ_{eff}. These parameters remain fixed throughout the 7-day replay, while the remaining physical parameters are taken from the literature. Figure 5 shows the 660 ft $\times$ 460 ft experimental field and the deployment locations of the buried node and aboveground gateways.

Comparison Methods: We compare Kairos with four categories of methods. **Static** selects the optimal polarization direction at initialization and keeps it fixed throughout the experiment. The periodic baselines, inspired by Demeter [17], recalibrate every 12, 24, or 48 hours and attempt to reduce the SF when the current SNR permits, denoted by **Periodic-12h**, **Periodic-24h**, and **Periodic-48h**. The VWC-triggered baselines recalibrate when the VWC change exceeds 0.2%, 0.4%, 0.8%, or 1.6%, denoted by **VWC-0.2%**, **VWC-0.4%**, **VWC-0.8%**, and **VWC-1.6%**. Finally, **Oracle** provides a theoretical lower bound by assuming future channel knowledge and selecting the energy-optimal action without probing overhead. Its future information is used only to compute the bound and is unavailable to Kairos or the online baselines.

In Kairos, the polarization front end consumes about 600 μW, while the RF splitter and hybrid coupler are passive. This overhead is negligible compared with mW-level data transmission. Moreover, both data and probing packets open two receive windows, and their energy is included in the corresponding transmission and calibration costs. Finally, other sensing, MCU, and radio-startup overheads are shared across methods and are therefore excluded from the comparison.

B. Overall Performance

We use the 7-day link traces under the default transceiver settings to evaluate the overall performance. In our emulation, data packets are generated periodically at an interval of 1 hour (i.e., 3,600 seconds). The frequency band is 904.1 MHz, the same as in our link data collection. BW, SF, TP, and payload are set to 125 kHz, 10, 2 dBm, and 20 bytes, respectively. In Kairos, we set the calibration cycle as one packet (n=1), preserving the model's agility in capturing temporal link opportunities and improving energy efficiency.

Result: As shown in Figure 6(a), Kairos achieves an accumulated energy cost of 24.22 mJ after 7 days, substantially lower than all online baselines. Compared to Static, Kairos reduces energy cost by 6.41$\times$ and closely approaches Oracle, which achieves 13.60 mJ with future channel knowledge and no probing energy. Compared with Periodic-12h, Periodic-24h, and Periodic-48h, Kairos reduces energy cost by 2.10$\times$, 1.75$\times$, and 3.71$\times$, respectively. The periodic methods end with 75.10 mJ, 66.70 mJ, and 114.08 mJ, indicating that a fixed calibration interval cannot consistently balance probing overhead and timely recalibration. Kairos also outperforms VWC-0.2%, VWC-0.4%, VWC-0.8%, and VWC-1.6% by

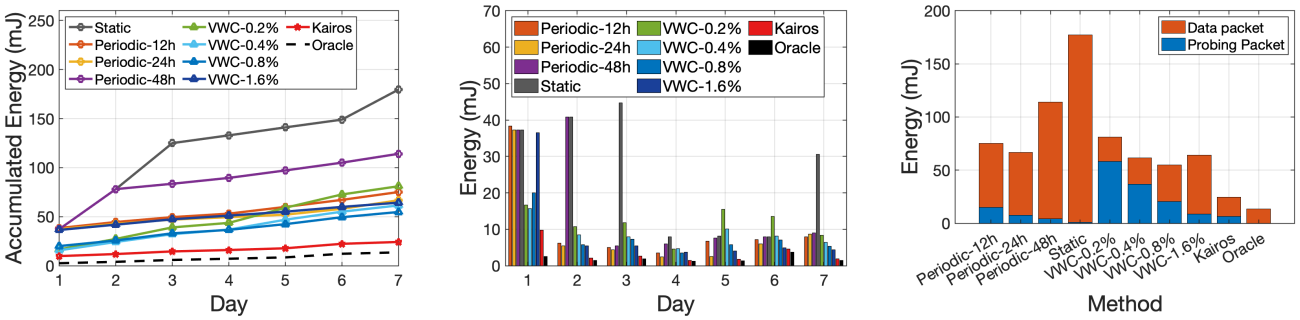

(a) Accumulated Energy (b) Energy per Day (c) Energy Types

Fig. 6: Overall performance of Kairos.

2.34×, 1.54×, 1.26×, and 1.65×, respectively. These results demonstrate the superior energy efficiency of Kairos under dynamic soil conditions. Kairos balances mismatch loss and probing overhead by triggering calibration when the predicted recoverable gain can reduce data-transmission energy, while history-guided search minimizes the required probes.

Furthermore, Figure 6(b) presents the day-by-day energy consumption. Kairos achieves the lowest energy among all online methods on each day and remains close to Oracle. The small gap to Oracle, which uses the optimal polarization without probing, indicates that prediction errors have limited impact on Kairos's decisions. The only noticeable increase in Kairos's daily energy occurs on Day 6, where it consumes 4.56 mJ. This increase is caused by rainfall-induced SNR degradation before the moisture change reached the sensor depth, which temporarily reduced the effectiveness of margin-based scheduling. In comparison, Static exhibits large energy spikes on Day 3 and Day 7, reaching 44.66 mJ and 30.56 mJ, respectively. Periodic methods also show unstable daily energy costs. Periodic-48h consumes 40.81 mJ on Day 2 due to delayed recalibration, while Periodic-12h and Periodic-24h incur high energy costs on Day 1 because of unnecessary probing. VWC-triggered methods mitigate some of these spikes, but their performance varies significantly with the selected threshold. For example, VWC-0.2% consumes 15.44 mJ and 13.55 mJ on Days 5 and 6, whereas VWC-1.6% reaches 36.47 mJ on Day 1. These results demonstrate that Kairos provides more stable daily energy efficiency than both fixed-period and fixed-threshold scheduling.

Figure 6(c) compares the probing and data-packet energy across different methods. Kairos spends only 6.49 mJ on probing while keeping data-packet energy at 18.08 mJ, achieving the best balance among all online methods. Its probing overhead is much lower than aggressive strategies such as Periodic-12h and VWC-0.2%, while its data energy is also substantially lower than Static and most threshold-based methods. Oracle has no probing energy because it assumes future channel knowledge and does not send probing packets. In comparison, periodic and VWC-triggered methods show clear tradeoffs. Reducing calibration frequency or using a larger VWC threshold lowers probing overhead but increases data-packet energy due to delayed recalibration. Conversely, frequent calibration reduces data energy but incurs higher probing overhead. These results show that Kairos more effectively balances calibration overhead and transmission efficiency.

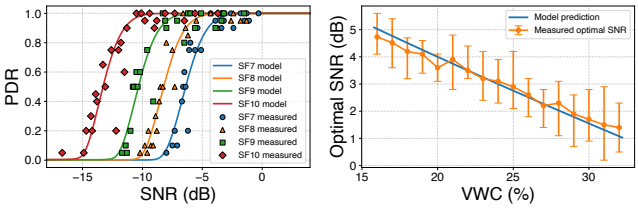

(a) Validation of Threshold-based Energy Estimation Model. (b) Validation of Margin Prediction Model.

Fig. 7: The model validation via ablation experiments.

TABLE II: Margin-prediction errors across varying deployment conditions.

Evaluation condition	MAE (dB)	RMSE (dB)
Overall	0.18	0.21
Across days	0.06–0.24	0.07–0.26
Across depths	0.08–0.14	0.11–0.17
Across link distances	0.11–0.16	0.12–0.16

C. Model Validation

We first evaluate whether the two models used by Kairos can accurately support calibration decisions. Figure 7(a) compares the measured PDR with the corrected PDR model under different spreading factors. Across SF7–SF10, the measured points closely match the model predictions, especially around the transition region where PDR changes rapidly with SNR. This result is important because Kairos uses this model to determine whether an estimated SNR gain can reduce transmission energy by enabling a lower spreading factor.

For the margin prediction model, we calibrate the effective soil conductivity as $\sigma_{\text{eff}} = 0.005 + 0.1\,\text{VWC}$ using the independent control-day dataset and keep this relationship fixed throughout the evaluation. Figure 7(b) compares the predicted and measured polarization-optimized SNR across VWC levels. Their close agreement shows that VWC provides a reliable prior for estimating the post-calibration SNR envelope, rather than the instantaneous SNR under a fixed polarization state. Table II reports prediction errors across days, burial depths, and link distances. The consistently low errors, together with the small gap between Kairos and Oracle in Figure 6(b), indicate that margin-prediction errors have limited impact on the final calibration and SF decisions.

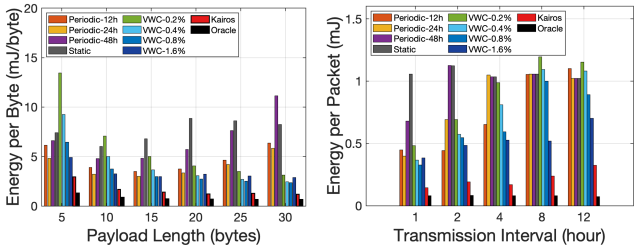

(a) Various Payload Length (b) Various Transmission Interval

Fig. 8: Energy cost under various parameters.

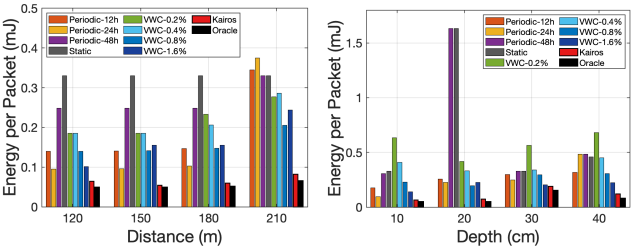

(a) Various Distance (b) Various Depth

Fig. 9: Energy cost under various locations.

D. Different Payload Length

To evaluate the impact of payload length on Kairos performance, we compute the energy costs of different methods across varying payload lengths.

Result: As shown in Figure 8(a), Kairos achieves the lowest energy among all online methods, with larger gains as payload size increases. At 30 bytes, it reduces energy by 4.38×, 3.95×, and 8.41× over Periodic-12h, Periodic-24h, and Periodic-48h, and by 1.63×, 1.07×, 0.99×, and 1.43× over VWC-0.2%, VWC-0.4%, VWC-0.8%, and VWC-1.6%, respectively. This advantage grows because probing overhead remains nearly constant, while transmission costs increase with payload length. By maintaining a reliable lower-SF link, Kairos becomes especially beneficial for larger packets.

E. Different Transmission Interval

To investigate the impact of transmission interval on Kairos performance, we simulate the scheduling outcomes of various methods across different transmission intervals and record the energy cost per transmission.

Result: As shown in Figure 8(b), Kairos achieves the lowest per-packet energy among all online methods across transmission intervals. At a 12-hour interval, it reduces energy by 2.38×, 2.15×, and 2.15× over Periodic-12h/24h/48h, respectively. Periodic methods incur higher cost when calibration frequently overlaps with data transmissions; for example, Periodic-12h calibrates before every packet at this interval. Kairos also reduces energy by 2.55×, 2.33×, 1.75×, and 1.16× over VWC-0.2%/0.4%/0.8%/1.6%, respectively. These results show that Kairos remains energy-efficient across different transmission intervals.

F. Different Horizontal Distance

As illustrated in Figure 5, we conducted experiments at multiple horizontal distances ranging from 60 m to 210 m.

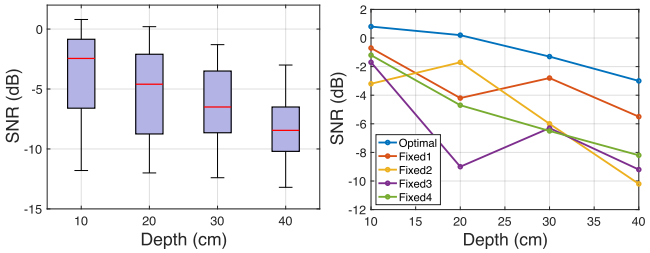

(a) SNR variation (b) Various polarization direction

Fig. 10: SNR distribution under various depths.

The orange triangles denote the gateway positions at various distances, while the blue star marks the location of the buried node, which is placed at a depth of 40 cm.

Result: Figure 9(a) compares the scheduling energy cost under different transmission distances. Kairos achieves the lowest energy among all online methods across all distances, with a more pronounced advantage at longer distances. At 210 meters, Kairos reduces energy cost by 3.22×, 3.59×, and 3.04× compared to Periodic-12h, Periodic-24h, and Periodic-48h, respectively. At the same distance, Periodic-12h and Periodic-24h show sharp energy increases, even exceeding Periodic-48h and Static, because long-distance links are more sensitive to SNR degradation and inefficient recalibration decisions. Kairos also outperforms VWC-triggered methods, reducing energy cost by 2.39×, 2.50×, 1.51×, and 1.98× compared to VWC-0.2%, VWC-0.4%, VWC-0.8%, and VWC-1.6%, respectively. These results demonstrate the superior energy efficiency of Kairos under different transmission distances.

G. Different Soil Depth

To validate the applicability of Kairos across different soil depths, we placed the node at four depths: 10 cm, 20 cm, 30 cm, and 40 cm, with the SF configured from 7 to 10.

Result: Figure 9(b) compares the scheduling energy cost across different burial depths. Kairos consistently achieves low energy consumption at all depths and remains close to Oracle. Notably, at 20 cm, Periodic-48h and Static incur much higher energy costs than other methods. Kairos reduces the energy cost by 2.46×, 2.03×, and 21.01× compared to Periodic-12h, Periodic-24h, and Periodic-48h, respectively. Kairos also outperforms VWC-triggered methods across different depths. At 20 cm, Kairos reduces the energy cost by 4.62×, 3.48×, 1.64×, and 2.03× compared to VWC-0.2%, VWC-0.4%, VWC-0.8%, and VWC-1.6%, respectively. The unusually high costs of Static and Periodic-48h at 20 cm result from the large temporal SNR variation shown in Figure 10(b). Static keeps the initial polarization direction, while Periodic-48h can remain misaligned for up to 48 hours. This persistent mismatch increases the selected SF and retransmission cost, whereas Kairos adapts before the loss persists.

As shown in Figure 10(a), the SNR peak decreases with burial depth due to stronger soil absorption. However, the magnitude of temporal and polarization-dependent SNR variation is not monotonic with depth. Figure 10(b) shows that the 20 cm link exhibits particularly large variation, likely due to local soil

heterogeneity and depth-dependent reflection, refraction, and scattering. This highlights the complex propagation dynamics of cross-soil links: greater depth lowers the overall SNR envelope but does not necessarily reduce polarization-induced variation. Kairos accommodates this variability through adaptive calibration and transmission control.

The evaluated range covers typical agricultural and environmental sensing deployments while preserving observable polarization variation. At greater depths, stronger attenuation may push the link into a low-SNR regime where polarization gains have less influence on transmission decisions.

V. Related Work

A. Wireless Underground Sensor Networks

Research on Wireless Underground Sensor Networks (WUSNs) has mainly addressed severe path loss and channel variability caused by soil heterogeneity. Peplinski et al. [31] established a widely used soil dielectric model, while later studies explored low-frequency EM and magnetic-induction communication [40]. Compared to ad-hoc WUSN, we focus on cross-soil LPWAN, a parallel IoT paradigm. Recent studies have demonstrated the advantages of LoRa-based WUSNs, leveraging its long-range capability and robust modulation scheme for underground applications [10], [16], [17]. Kairos focuses specifically on reducing the communication and calibration energy of cross-soil LoRa links through joint polarization and transmission control.

B. Polarization-aware Communication for IoT

Polarization-aware communication has been explored in IoT systems to mitigate link degradation caused by polarization mismatch. LLAMA [41] uses a reconfigurable metasurface to dynamically adjust signal polarization and mitigate polarization mismatch. Polartracker [42] and Polarscheduler [43] further model polarization variations in floating LoRa networks and schedule transmissions during favorable alignment. In contrast, Kairos targets irregular and unpredictable polarization variations in cross-soil LoRa networks through soil-aware transmission control.

C. Adaptive Data Rate and Transmission Control in LoRa

Adaptive Data Rate (ADR) improves LoRa and LPWAN scalability and energy efficiency by adjusting transmission parameters to link conditions, thereby reducing airtime, collisions, and device energy consumption [44]–[46]. For underground links, moisture-aware methods further adapt link configurations to compensate for moisture-induced attenuation [16], but typically assume a fixed antenna state and overlook recoverable polarization mismatch. Kairos complements these methods by incorporating polarization alignment into transmission control.

Unlike conventional ADR, polarization calibration incurs explicit probing overhead. Kairos uses VWC to estimate polarization-optimized link quality and triggers calibration when the predicted recoverable margin can reduce data-transmission energy, while minimizing the probing overhead during the polarization calibration.

VI. Discussion

Calibration Cycle Setting. The length of the calibration cycle is determined by the number of data transmissions. A short calibration cycle keeps the agility for temporal channel changes by allowing more frequent calibration decisions, but increases computation at the gateway, especially when serving multiple nodes. Saying that, when the cross-soil channel remains stable after a suitable polarization state has been established, different cycle lengths incur similar probing overhead because no further calibration benefit arises. However, selecting a longer calibration cycle can further reduce the computation overhead while maintaining the energy efficiency of data transmission. In that case, nodes and gateways also need extra cost to accurately predict when a stable cross-soil channel will appear. In the current Kairos design, we conservatively set $n = 1$ to keep the agility, accepting the additional gateway-side computation while keeping nodes lightweight.

Generality. Our evaluation is limited to a single soybean field and does not cover different soil types, crops, or seasons. However, Kairos's control logic remains unchanged across sites, deployment at a new site only requires recalibrating the two soil-dependent parameters, Δ_{soil} and σ_{eff}.

Multi-node Scalability. Multiple nodes will bring more computation burden for a gateway and may incur the risk of packet collision without scheduling. Since agricultural sensing deployments are often sparse, this limitation is less restrictive for our target scenario. Denser deployments can incorporate gateway scheduling and randomized backoff to reduce probe–feedback contention.

VII. Conclusion

In this paper, we presented Kairos, a polarization-aware transmission control framework that explicitly integrates antenna polarization into energy-aware LoRa transmission control. By formulating energy efficiency as a long-term optimization problem, Kairos jointly considers transmission cost and calibration overhead. It introduces a threshold-based energy estimation model and a margin prediction model to determine when polarization calibration is energy beneficial, an efficient polarization search strategy to reduce probing overhead, and a polarization-aware transmission mechanism that remains compatible with existing LoRa control paradigms. We implemented Kairos on commercial off-the-shelf LoRa devices and evaluated it in a real agricultural field deployment. Experimental results demonstrate that Kairos can reduce energy consumption by up to $3.71\times$ compared to state-of-the-art approaches, while maintaining reliable cross-soil communication under dynamic environmental conditions.

Acknowledgement

We sincerely thank the anonymous reviewers for their valuable feedback. This work was partially supported by NSF CAREER Award 2338976.

REFERENCES

[1] D. Vasisht, Z. Kapetanovic, J. Won, X. Jin, R. Chandra, S. Sinha, A. Kapoor, M. Sudarshan, and S. Stratman, "Farmbeats: an iot platform for data-driven agriculture," in *USENIX NSDI*, 2017.

[2] Y. Liu, M. Gan, H. Zeng, L. Liu, Y. Dong, and Z. Cao, "Hydra: Accurate multi-modal leaf wetness sensing with mm-wave and camera fusion," in *ACM MobiCom*, 2024, pp. 800–814.

[3] Y. Liu, M. Gan, G. Li, Y. Dong, and Z. Cao, "Adonis: Neural-enhanced fine-grained leaf wetness sensing with efficient mmwave imaging," in *IEEE INFOCOM*, 2025, pp. 1–10.

[4] Y. Liu, M. Gan, H. Zeng, Y. Ren, G. Li, J. Lin, Y. Dong, X. Tan, and Z. Cao, "Proteus: Enhanced mmwave leaf wetness detection with cross-modality knowledge transfer," in *ACM SenSys*, 2025, pp. 43–57.

[5] S. I. Siam, H. Ahn, L. Liu, S. Alam, H. Shen, Z. Cao, N. Shroff, B. Krishnamachari, M. Srivastava, and M. Zhang, "Artificial intelligence of things: A survey," *ACM Transactions on Sensor Networks*, vol. 21, no. 1, pp. 1–75, 2025.

[6] J. Bayar, N. Ali, Z. Cao, Y. Ren, and Y. Dong, "Artificial intelligence of things (aiot) for precision agriculture: Applications in smart irrigation, nutrient and pest management," *Smart Agricultural Technology*, p. 101629, 2025.

[7] A. Pagano, D. Croce, I. Tinnirello, and G. Vitale, "A survey on lora for smart agriculture: Current trends and future perspectives," *IEEE Internet of Things Journal*, vol. 10, no. 4, pp. 3664–3679, 2022.

[8] S. J. Ramson, W. D. León-Salas, Z. Brecheisen, E. J. Foster, C. T. Johnston, D. G. Schulze, T. Filley, R. Rahimi, M. J. C. V. Soto, J. A. L. Bolivar *et al.*, "A self-powered, real-time, lorawan iot-based soil health monitoring system," *IEEE Internet of Things Journal*, vol. 8, no. 11, pp. 9278–9293, 2021.

[9] A. R. Silva and M. C. Vuran, "Communication with aboveground devices in wireless underground sensor networks: An empirical study," in *IEEE ICC*, 2010.

[10] B. Zhou, V. S. S. L. Karanam, and M. C. Vuran, "Impacts of soil and antenna characteristics on lora in internet of underground things," in *IEEE GLOBECOM*, 2021.

[11] L. Aldhaheri, N. Alshehhi, I. I. J. Manzil, R. A. Khalil, S. Javaid, N. Saeed, and M.-S. Alouini, "Lora communication for agriculture 4.0: Opportunities, challenges, and future directions," *IEEE Internet of Things Journal*, vol. 12, no. 2, pp. 1380–1407, 2024.

[12] Y. Ren, A. Gamage, L. Liu, M. Li, S. Chen, Y. Dong, and Z. Cao, "Sateriot: High-performance ground-space networking for rural iot," in *ACM MobiCom*, 2024.

[13] Y. Ren, L. Liu, C. Li, Z. Cao, and S. Chen, "Is lorawan really wide? fine-grained lora link-level measurement in an urban environment," in *IEEE ICNP*, 2022.

[14] S. Tong, J. Wang, J. Yang, Y. Liu, and J. Zhang, "Citywide lora network deployment and operation: Measurements, analysis, and implications," in *ACM SenSys*, 2023.

[15] J. C. Liando, A. Gamage, A. W. Tengourtius, and M. Li, "Known and unknown facts of lora: Experiences from a large-scale measurement study," *ACM Transactions on Sensor Networks*, vol. 15, no. 2, pp. 1–35, 2019.

[16] K. Lin and T. Hao, "Experimental link quality analysis for lora-based wireless underground sensor networks," *IEEE Internet of Things Journal*, vol. 8, no. 8, pp. 6565–6577, 2020.

[17] Y. Ren, W. Sun, J. Du, H. Zeng, Y. Dong, M. Zhang, S. Chen, Y. Liu, T. Li, and Z. Cao, "Demeter: Reliable cross-soil lpwan with low-cost signal polarization alignment," in *ACM MobiCom*, 2024, pp. 230–245.

[18] Y. Li, J. Yang, and J. Wang, "Dylora: Towards energy efficient dynamic lora transmission control," in *IEEE INFOCOM*, 2020.

[19] C. Li and Z. Cao, "Lora networking techniques for large-scale and long-term iot: A down-to-top survey," *ACM Computing Surveys (CSUR)*, vol. 55, no. 3, pp. 1–36, 2022.

[20] J. Du, Y. Ren, Z. Zhu, C. Li, Z. Cao, Q. Ma, and Y. Liu, "Srlora: Neural-enhanced lora weak signal decoding with multi-gateway super resolution," in *MobiHoc*, 2023, pp. 270–279.

[21] J. Du, Y. Liu, Y. Ren, L. Liu, and Z. Cao, "Loratrimmer: Optimal energy condensation with chirp trimming for lora weak signal decoding," in *ACM MobiCom*, 2024, pp. 1104–1118.

[22] K. Nguyen, Y. Ren, J. Du, J. Lin, M. Gan, S. Chen, M. Zhang, C. Peng, and Z. Cao, "Loraseek: Boosting denoising ability in neural-enhanced lora decoder via hierarchical feature extraction," in *ACM MobiCom*, 2025, pp. 712–726.

[23] Y. Ren, P. Cai, J. Jiang, J. Du, and Z. Cao, "Prism: High-throughput lora backscatter with non-linear chirps," in *IEEE INFOCOM*, 2023, pp. 1–10.

[24] C. Li, Y. Ren, S. Tong, S. I. Siam, M. Zhang, J. Wang, Y. Liu, and Z. Cao, "Chirptransformer: Versatile lora encoding for low-power wide-area iot," in *ACM MobiSys*, 2024, pp. 479–491.

[25] Y. Ren, G. Li, Y. Liu, Y. Dong, and Z. Cao, "Aeroecho: Towards agricultural low-power wide-area backscatter with aerial excitation source," in *IEEE INFOCOM*, 2025, pp. 1–10.

[26] F. Cuomo, M. Campo, A. Caponi, G. Bianchi, G. Rossini, and P. Pisani, "Explora: Extending the performance of lora by suitable spreading factor allocations," in *IEEE WiMob*, 2017.

[27] A. Gamage, J. Liando, C. Gu, R. Tan, M. Li, and O. Seller, "Lmac: Efficient carrier-sense multiple access for lora," *ACM Transactions on Sensor Networks*, vol. 19, no. 2, pp. 1–27, 2023.

[28] J. Lin, R. Xiong, Z. Xu, W. Tian, C. Chen, X. Dong, and J. Luo, "Multi-node concurrent localization in lora networks: Optimizing accuracy and efficiency," in *IEEE INFOCOM*, 2024.

[29] Semtech, "SX1276-7-8-9 Datasheet," 2020, accessed: 2026-06-05. [Online]. Available: https://semtech.my.salesforce.com/sfc/p/#E0000000JelG/a/2R0000001Rbr/6EfVZUorrpoKFfvaF_Fkpgp5kzjiNyiAbqcpqh9qSjE

[30] T. Elshabrawy and J. Robert, "Closed-form approximation of lora modulation ber performance," *IEEE Communications Letters*, vol. 22, no. 9, pp. 1778–1781, 2018.

[31] N. R. Peplinski, F. T. Ulaby, and M. C. Dobson, "Dielectric properties of soils in the 0.3-1.3-ghz range," *IEEE transactions on Geoscience and Remote sensing*, vol. 33, no. 3, pp. 803–807, 1995.

[32] H. Huang, J. Shi, F. Wang, D. Zhang, and D. Zhang, "Theoretical and experimental studies on the signal propagation in soil for wireless underground sensor networks," *Sensors*, vol. 20, no. 9, p. 2580, 2020.

[33] J. Kiefer, "Sequential minimax search for a maximum," *Proceedings of the American mathematical society*, vol. 4, no. 3, pp. 502–506, 1953.

[34] Dragino, "Lps8 indoor lorawan gateway," accessed: May 20, 2026. [Online]. Available: https://www.dragino.com/products/lora-lorawan-gateway/item/148-lps8.html=

[35] DRAGINO, "Dragino lora shield v1.4," accessed: May 20, 2026. [Online]. Available: https://www.zagroselec.ir/STFiles/GetAppDocument/1/True/279c1ecf-4b05-4d5a-babe-1ef6c973ead9.pdf

[36] PINO-TECH, "Soilwatch 10 – soil moisture sensor," accessed: May 20, 2026. [Online]. Available: https://pino-tech.eu/soilwatch10/

[37] XRDS-RF, "3db xrds-rf 698-2700mhz passive splitter," accessed: May 20, 2026. [Online]. Available: https://www.amazon.com/Wide-Band-Splitter-3dB-Type-Female-50-XRDS-RF/dp/B07V6YH8BV

[38] pSemi, "pe44820," accessed: May 20, 2026. [Online]. Available: https://www.psemi.com/products/rf-phase-amplitude-control/phase-shifters/pe44820

[39] WAVEFORM, "2×2 cross-polarized 600-2700 mhz outdoor antenna," accessed: May 20, 2026. [Online]. Available: https://www.waveform.com/products/2x2-mimo-outdoor-panel-antenna

[40] Z. Sun and I. F. Akyildiz, "Channel modeling and analysis for wireless networks in underground mines and road tunnels," *IEEE Transactions on communications*, vol. 58, no. 6, pp. 1758–1768, 2010.

[41] L. Chen, W. Hu, K. Jamieson, X. Chen, D. Fang, and J. Gummeson, "Pushing the physical limits of iot devices with programmable metasurfaces," in *USENIX NSDI*, 2021.

[42] Y. Wang, X. Zheng, L. Liu, and H. Ma, "Polartracker: Attitude-aware channel access for floating low power wide area networks," in *IEEE INFOCOM*, 2021.

[43] X. Zheng, R. Li, Y. Wang, L. Liu, and H. Ma, "Polarscheduler: Dynamic transmission control for floating lora networks," *ACM Transactions on Sensor Networks*, vol. 20, no. 3, pp. 1–33, 2024.

[44] J. Finnegan, R. Farrell, and S. Brown, "Analysis and enhancement of the lorawan adaptive data rate scheme," *IEEE Internet of Things Journal*, vol. 7, no. 8, pp. 7171–7180, 2020.

[45] C. Jiang, Y. Yang, X. Chen, J. Liao, W. Song, and X. Zhang, "A new-dynamic adaptive data rate algorithm of lorawan in harsh environment," *IEEE Internet of Things Journal*, vol. 9, no. 11, pp. 8989–9001, 2021.

[46] N. Alshaer, Z. Reda, and S. Napoleon, "Enhanced adaptive data rate and power control for resilient and energy-efficient lorawan," *IEEE Internet of Things Journal*, 2025.